Journal of Volcanology and Geothermal Research 405 (2020) 107047

Contents lists available at ScienceDirect

Journal of Volcanology and Geothermal Research

journal homepage: www.elsevier.com/locate/jvolgeores

Harmonic ionospheric oscillation by the 2010 eruption of the Merapi volcano, Indonesia, and the relevance of its amplitude to the mass eruption rate

Mokhamad Nur Cahyadi [a,*], Ririn Wuri Rahayu [a], Kosuke Heki [b], Yuki Nakashima [c]

[a] Dept. Geomatic Engineering, Institut Teknologi Sepuluh Nopember (ITS) Surabaya, Surabaya, Indonesia
[b] Dept. Earth Planet. Sci., Hokkaido University, Sapporo, Japan
[c] Earthquake Res. Inst. Univ. Tokyo, Tokyo, Japan

ARTICLE INFO

Article history:
Received 22 November 2019
Received in revised form 28 August 2020
Accepted 2 September 2020
Available online 3 September 2020

Keywords:
GNSS-TEC
Ionospheric disturbance
Plinian eruption
Indonesia
Merapi
Kelud
Calbuco

ABSTRACT

Using continuous data from ground-based Global Satellite Navigation System (GNSS) receivers in Java and Sumatra, Indonesia, we studied the response of ionospheric total ionospheric electron content (TEC) to the 2010 Nov.5 eruption of the Merapi volcano in central Java. We then compared the results with the case of the 2014 Feb.13 eruption of the Kelud volcano, eastern Java. The TEC showed a quasi-periodic oscillation of a frequency ~4 mHz with average amplitudes of 0.9 and 1.8% relative to background values lasting for ~20 and ~ 120 min for the Merapi and Kelud eruptions, respectively. By comparing the two cases, together with the 2015 April eruption of the Calbuco volcano, Chile, we found the relative TEC oscillation amplitude may scale with the mass eruption rate. This suggests that the product of such TEC oscillation amplitude and the duration provides a new measure for the total volume of the volcanic deposits.

1. Introduction

Explosive volcanic eruptions make severe atmospheric perturbations like blast or infrasound. They are often detected by barometers or microphones installed on the ground (e.g. Dabrowa et al., 2011; Matoza et al., 2019). Infrasound monitoring is vital to detect eruptions from the far-field and/or during the nighttime. Such infrasounds are typically monitored with barometers or microphones installed on the ground, enabling us to infer acoustic energy using shock waves and frequency contents. However, it is difficult to detect the acoustic energy propagating to upper atmospheric layers with these conventional instruments.

Such acoustic disturbances are also detected as perturbations in the ionosphere. The ionosphere is the ionized region of the Earth's upper atmosphere and ranges from ~60 to over 1000 km above ground. It shows diurnal variation governed by solar radiation and is often disturbed by solar and geomagnetic activities. Ionospheric disturbances occur also by activities below, such as earthquakes, tsunamis, and volcanic eruptions. The ionospheric total electron content (TEC) is easily measured with dual-frequency receivers of the Global Satellite Navigation System (GNSS) such as Global Positioning System (GPS) (e.g. Hofmann-Wellenhof et al., 2008). Continuous observation with dense GNSS networks are useful to study such ionospheric disturbances (Fig. 1).

In addition to ionospheric disturbances by large earthquakes (e.g. Heki, 2020) and tsunamis (e.g. Occhipinti et al., 2013), those by volcanic eruptions have been reported (e.g. Astafyeva, 2019). Heki (2006) used the GPS-TEC technique to study the ionospheric response to the Vulcanian explosion of Asama volcano, central Japan, on September 1, 2004. TEC showed transient N-shaped disturbances of a period 1–2 min, ~10 min after the explosion. Such a TEC change occurs when the acoustic wave excited by the explosion arrives at the ionospheric F region (altitude ~300 km) and make electron density anomalies there (Fig. 1 left). The disturbance propagates mainly toward the equator, due to interaction of the ambient geomagnetic fields, with the acoustic wave speed in the F region. For the 2004 Asama eruption, Heki (2006) estimated the explosion energy by comparing the TEC disturbance amplitude with an artificial explosion with known energy (Calais et al., 1998). Nakashima (2018) also studied TEC disturbance signals after the 2015 eruption of the Kuchinoerabujima Volcano, south of Kyushu, Japan.

In contrast to such explosive eruptions, harmonic oscillations of TEC of ~4 mHz often emerge from strong continuous eruptions (Fig. 1 right). For example, an oscillation of TEC lasted for ~2 h associated with the

* Corresponding author.
E-mail address: cahyadi@geodesy.its.ac.id (M.N. Cahyadi).

https://doi.org/10.1016/j.jvolgeores.2020.107047
0377-0273/

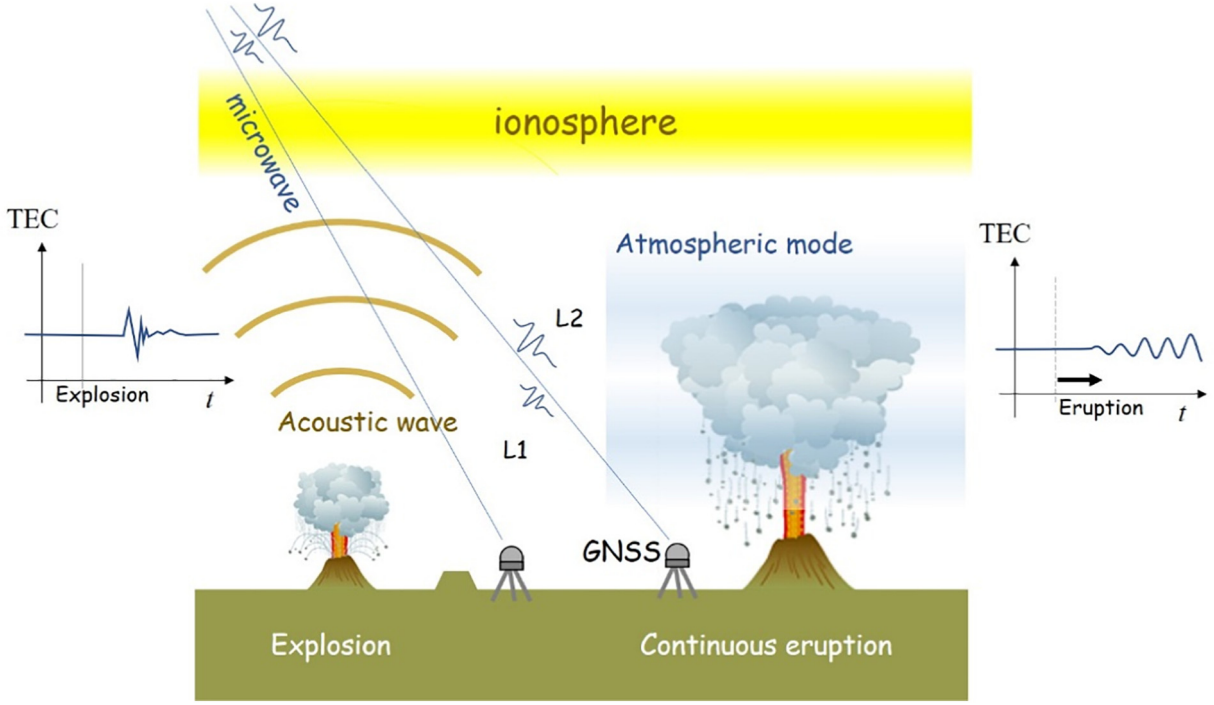

Fig. 1. Ionospheric disturbance caused by explosive (left) and continuous (right) volcanic eruptions can be detected by differential ionospheric delays of microwave signals in two carrier frequencies from GNSS satellites. Explosive eruptions often cause transient disturbances in ionosphere while continuous eruptions sometimes excite atmospheric modes and continuous oscillatory disturbances in ionosphere.

2003 eruption of the Soufrière Hills volcano, Montserrat, as reported by Dautermann et al. (2009a, 2009b). Nakashima et al. (2016) used GNSS receivers in Indonesia to analyze the TEC response to the 2014 February Plinian eruption of the Kelud volcano eastern Java, Indonesia. They reported resonant oscillations of TEC lasting for ~2 h. Later, Shults et al. (2016) reported similar TEC oscillations lasting ~1.5 and ~ 6 h during the two Plinian eruption episodes on 22 and 23 April 2015, of the Calbuco volcano, Chile.

GNSS-TEC technique has been applied to study coseismic ionospheric disturbances for tens of cases (Heki, 2020). Like volcanic eruptions, they are characterized by N-shaped disturbances propagating as acoustic waves with magnitude-dependent amplitudes (Cahyadi and Heki, 2015). Acoustic waves propagating upward are bounced back, causing resonant oscillations in distinct frequencies (Tahira, 1995). Acoustic resonance in 3.7 and 4.4 mHz was found in background free-oscillations of the solid earth (Nishida et al., 2000), and these frequencies were identified in post-seismic monochromatic TEC oscillations by GPS-TEC after the 2004 Sumatra-Andaman earthquake (Choosakul et al., 2009), the 2011 Tohoku-oki earthquake (Rolland et al., 2011; Saito et al., 2011), and the 2007 Bengkulu earthquake (Cahyadi and Heki, 2013).

Harmonic oscillations, often observed during large continuous volcanic eruptions, are also due to such acoustic resonances of the atmosphere. Kanamori et al. (1994) found atmospheric resonance frequency components lasting >5 h in seismometer records after the 1991 eruption of the Pinatubo volcano, the Philippines, and Watada and Kanamori (2010) considered that harmonic ground oscillation is due to atmospheric resonance excited by continuous eruption of the volcano.

Here we present a new example of ionospheric disturbances by the 2010 Merapi eruption and compare the results with past examples, i.e. the 2014 Kelud eruption (Nakashima et al., 2016) and the 2015 Calbuco eruption (Shults et al., 2016), to better understand ionospheric disturbances by continuous volcanic eruptions. We also explore the possibility of ionospheric disturbances as new information to complement classical indices like Volcanic Explosivity Index (VEI).

2. Volcanic eruptions and GNSS data in Indonesia

Merapi volcano, central Java, Indonesia, erupted repeatedly with average intervals of 4–6 years. The 2010 eruption sequence of the Merapi volcano started after 4 years of quiescence with a phreatomagmatic blast on October 26. The activity peaked at midnight on November 4 (November 5 in local time) and lasted until July 15, 2012. This eruption sequence changed the summit morphology drastically (Surono et al., 2012) and is regarded as one of the most violent events of this volcano in its observation history. The details of this eruption sequence are available in articles included in the special issue of this journal (Jousset et al., 2013).

According to the eruptive timeline of the 2010 eruption compiled by Komorowski et al. (2013), the activity started as the non-eruptive stage 1 characterized by various kinds of unrest. Then, the phreatomagmatic blast on October 26 occurred as stage 2, and it is followed by stage 3 characterized by recurrent rapid dome growth and destruction explosion and collapse. The ionospheric signals discussed in this study are found around ~17:30 UT, November 4 (00:30 LT, November 5), shortly after the most intensive phase (stage 4). The stage 4 started at 17:02 UT, November 4 (00:02 LT, November 5), followed by a paroxysmal eruption lasting for ~10 min. The plume height reached 17 km during this stage (Carr et al., 2020). Then subsequent sub-Plinian eruption lasted for ~3 h (stages 5 and 6). VEI of the whole eruption sequence is recorded as 4.

We used data from 11 permanent tracking dual-frequency GNSS stations in the InaCORS (Indonesian Continuously Operating Reference Stations) network and IGS (International GNSS Service) network around the volcano (Fig. 2). The details of the methods to extract TEC from raw GNSS data are explained in Heki (2020). We converted the ionospheric linear combination, i.e. the phase

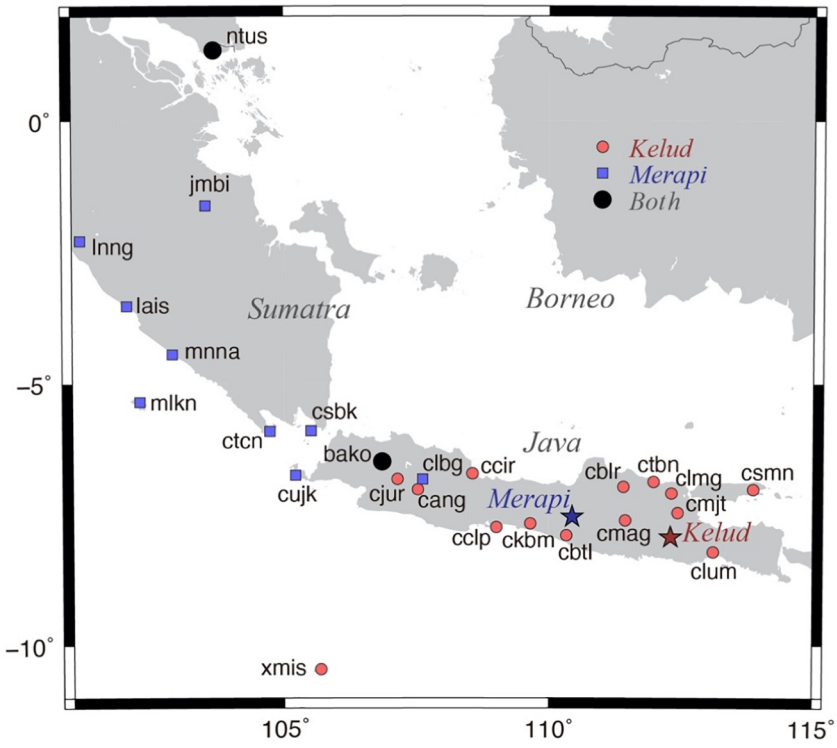

Fig. 2. GNSS stations used in this study in Java, Sumatra, and nearby islands. The Kelud volcano, Eastern Java, and the Merapi volcano, Central Java, are marked with the red and blue stars, respectively. Blue and red rectangles show GNSS stations used to study the Merapi and the Kelud eruptions, respectively. The two black circles show stations used for both cases. (For interpretation of the references to colour in this figure legend, the reader is referred to the web version of this article.)

differences of the two microwave carriers (L1: ~1.5 GHz and L2: ~1.2 GHz), into TEC. Fig. 3 shows examples of the TEC changes during 16–18 UT observed using ~10 different GPS satellites at two GNSS stations.

For the February 13, 2015, VEI 4 Plinian eruption of the Kelud volcano, eastern Java, Nakashima et al. (2016) performed GNSS-TEC studies using InaCORS and IGS stations around the volcano (Fig. 2). The climactic phase of this eruption started around 16:10–16:15 on that day, and the eruption column reached ~26 km above sea level, and the umbrella cloud laterally spread at a height of 18–20 km (Suzuki and Iguchi, 2019). The period of the TEC oscillation reported in Nakashima et al. (2016) occurred during this phase.

For comparison, we discuss ionospheric disturbances after the April 22–23, 2015, Calbuco volcano eruption reported in Shults et al. (2016). There we downloaded GNSS data from the Argentine GNSS network RAMSAC (Red Argentina de Monitoreo Satelital Continuo) (http://www.ign.gob.ar) and processed the data in the same way as the two other eruptions. The two Plinian eruption episodes on April 22 and 23 with TEC oscillations correspond to stages 3 and 4, respectively, of the eruption sequence compiled by Romero et al. (2016). The plume of these eruptions had the maximum height of 23 km above sea level (Van Eaton et al., 2016), and the VEI was recorded as 4.

Original TEC is the slant-TEC (STEC), number of electrons integrated along the line-of-sight (LoS) connecting satellites and receivers. They are usually expressed using TECU (TEC unit, 1 TECU $= 10^{16}$ el/m^2). After removing the inter-frequency bias using differential code bias (DCB) in the header information of Global Ionospheric Maps obtained from University of Berne, Switzerland (www.aiub.unibe.ch/download/) (satellite bias) and the receiver bias determined by minimum scalloping (Rideout and Coster, 2006), we convert STEC to vertical TEC (VTEC) by multiplying them with the cosine of the incidence angle of LoS at the ionospheric piercing point (IPP) with a hypothetical thin layer at the altitude of maximum ionization (300 km in this study). Propagation of ionospheric disturbances is represented by using the ground projection of IPP called sub-ionospheric points (SIP).

3. TEC oscillation and its propagation after the 2010 Merapi eruption

Fig. 3a shows TEC time series high-pass filtered by subtracting the best-fit polynomials with degrees 8 (Heki, 2020). The period within the two dashed vertical lines indicates the stage 4 of the 2010 Merapi eruption (17:02–17:13 UT) (Komorowski et al., 2013). Ionospheric TEC oscillations started shortly after the end of stage 4 (~17:20 UT) with GPS satellites 18 and 25 from the clbg station (Fig. 3a top) and with GPS satellite 29 from ntus (Fig. 3a bottom). The TEC oscillation has periods of 4–5 min. N-shaped disturbances are often seen after explosive volcanic eruptions (e.g. Heki, 2006), but these types of signals were not observed. Fig. 3b shows that SIP tracks of these satellites are located near the volcano. Fig. 4 shows that the observed peak frequency of the oscillation shown in Fig. 3 is consistent with the two atmospheric mode frequencies, 3.7 and 4.4 mHz, although the duration is not long enough to enable separation of the two peaks. Peaks seen for lower frequencies (1–2 mHz) would reflect the misfit of the polynomial reference curves to the observed STEC curves.

Fig. 5 shows snapshots of distribution of VTEC anomalies at 8 epochs during a 14-minutes period. Ionospheric anomalies emerged ~20 min after the start of the stage 4 eruption and alternating positive and negative wave crests propagate outward from the volcano. The stage 4 activity consists of laterally directed dome explosions over a period of 11 min which destroyed the rapidly emplaced lava dome (Komorowski et al., 2013). This would have excited acoustic waves propagating upward, and let standing waves in lower atmosphere grow large enough to make detectable harmonic oscillations in the ionosphere in 20 min. After this stage, stage 5 (dome collapse) and stage 6 (sub-Plinian eruption) lasted for ~3 h (Komorowski et al., 2013), but we do not find significant ionospheric disturbances during this period.

We estimated propagation velocity by plotting the time and distance from the volcano of the TEC disturbances as ~0.8 km s^{-1} (Fig. 6). This is consistent with that Nakashima et al. (2016) found for the 2014 Kelud eruption and corresponds to the acoustic

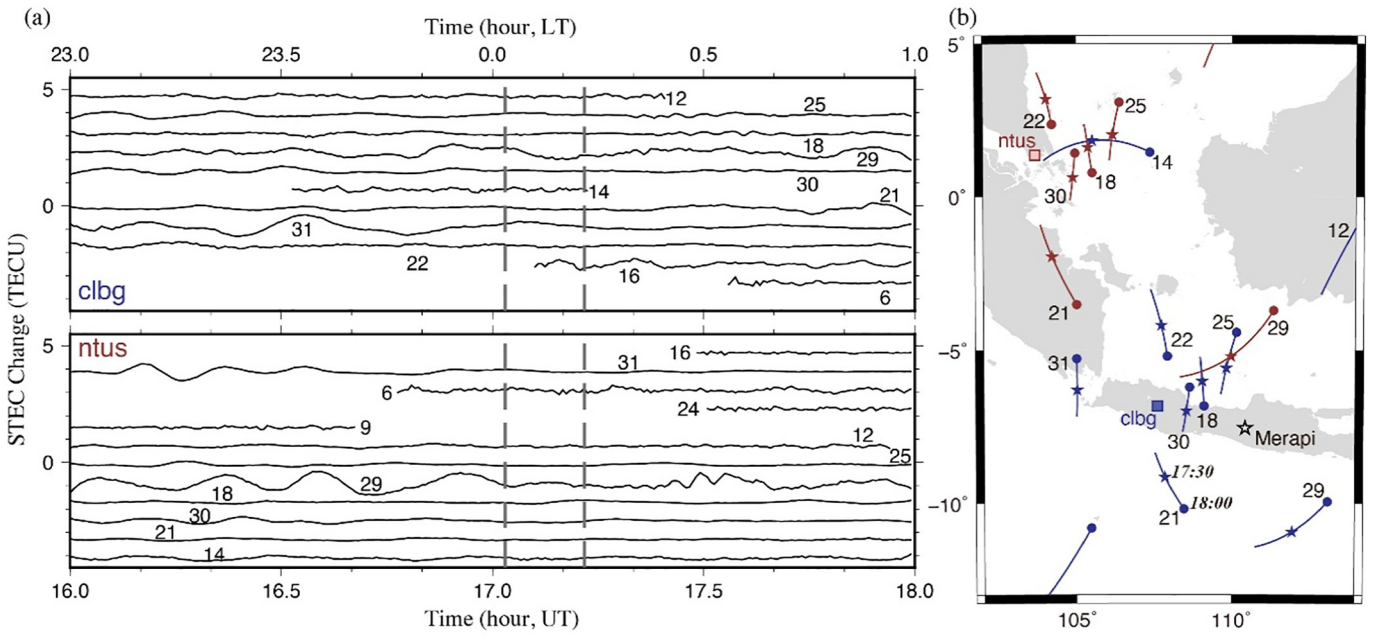

Fig. 3. (a) Time series 16.00–18.00 UT (23:00 to 01:00 in LT), Nov.5, 2010, of STEC changes observed at the two GNSS stations, clbg and ntus. The period within the two dashed vertical lines corresponds to the stage 4 of the 2010 Merapi eruption (17:02–17:13 UT) (Komorowski et al., 2013). Ionospheric TEC oscillations are seen 20 min after the eruption with satellites 25 and18 from clbg and with satellite 29 from ntus. (b) Trajectories of SIP for GPS satellites in 17.1–18.0 UT as seen from clbg (blue) and ntus (red) stations. On the trajectories, small stars indicate SIP at 17.5 UT, and filled circles indicate those at 18.0 UT. (For interpretation of the references to colour in this figure legend, the reader is referred to the web version of this article.)

wave speed in the F region of the ionosphere. Figs. 5 and 6 suggest that the TEC oscillation can be traced as far as 500–600 km from the volcano.

4. Comparison between the 2010 Merapi, 2014 Kelud, and 2015 Calbuco eruptions

4.1. Oscillation amplitudes

Next, we discuss the amplitudes of the observed resonant oscillation in VTEC anticipating that such amplitudes reflect the intensity of the continuous eruption. The observed amplitudes would, however, depend also on other factors such as distance from the volcano, the LoS incidence angles with the wave fronts, and the angle between the wave fronts and geomagnetic fields. The largest amplitudes of the electron density changes are expected to occur when the wave front of the neutral atmosphere is perpendicular to the geomagnetic field (Rolland et al., 2013). Also, a large amplitude occurs when LoS penetrates the wave front with a shallow angle.

Considering these points, we compared the VTEC oscillation amplitudes of the two Indonesian volcanoes using the satellite-station pairs with similar geometric conditions. For the 2015 Calbuco eruption, we used data with one GPS satellite (Sat.03) and two GLONASS (Russian GNSS) satellites (Sat.07R and 08R) during the first eruptive episode. We compare them in Fig. 7. For the Calbuco case, the observing time window is longer than the other cases and we see change in the oscillation amplitudes in time reflecting the changing distance between the volcano and the SIP. Also, between-satellite amplitude differences are caused by differences in geometry as explained above.

4.2. Index for total volume of deposit

From Fig. 7, stations with distance 200–300 km from the Merapi volcano after its 2014 eruption is shown to have an average peak-to-peak

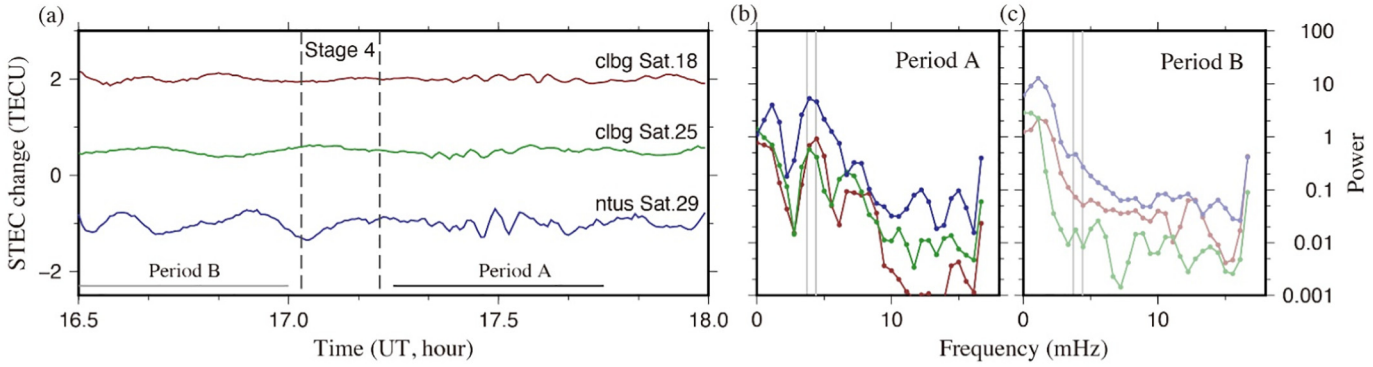

Fig. 4. (a) The high-pass filtered STEC time-series at clbg (GPS Sat. 18 and 25) and ntus (GPS Sat. 29) show monochromatic oscillation lasting ~20 min shortly after the stage 4 of the Merapi eruption. Two gray horizontal lines show time windows (Period A 17:15–17:45 UT, Period B 16:30–17:00) used for the spectral analyses of the two periods. (b) Period A shows peaks around 4 mHz, close to the two atmospheric resonance frequencies 3.7 and 4.4 mHz (two vertical lines in light gray), but (c) Period B does not show such peaks.

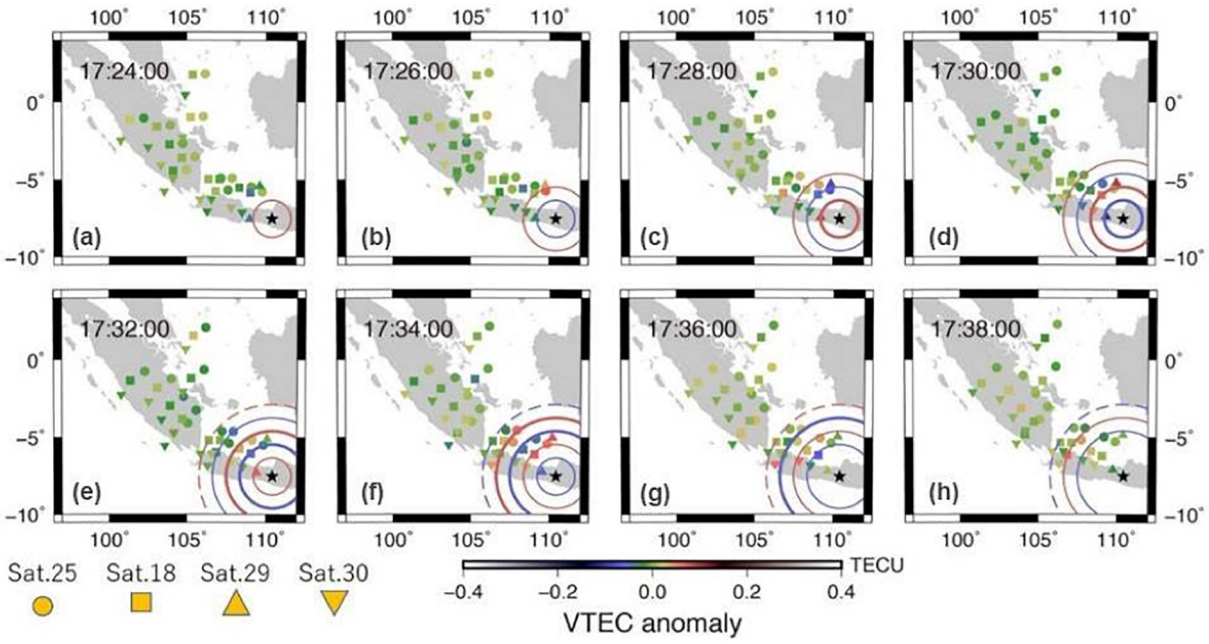

Fig. 5. Spatial distributions of the VTEC anomalies by the 2010 Merapi eruption at 8 epochs with 2-minutes time separation (epoch times given in UT). Red and blue circles correspond to positive and negative anomalies (values in Fig. 3 converted to VTEC), respectively. Circular wave crests are drawn assuming their expansion from the Merapi volcano by a velocity of ~0.8 km s^{-1}. (For interpretation of the references to colour in this figure legend, the reader is referred to the web version of this article.)

VTEC fluctuation of 0.10 ± 0.01 TECU. On the other hand, stations with similar distances from the Kelud volcano show the VTEC oscillations with amplitude of 0.73 ± 0.09 TECU (average over the first 20 min). The background VTEC in each eruption was ~11 and ~ 40 TECU for the 2010 Merapi and the 2015 Kelud eruptions, respectively. Then their amplitudes relative to background VTEC values are 0.91 ± 0.12% and 1.83 ± 0.23%, respectively. For the 2015 Calbuco case, the amplitude of oscillation was 0.23 ± 0.02 TECU and the background VTEC was ~26.0 TECU, and so the relative amplitude is 0.89 ± 0.09%.

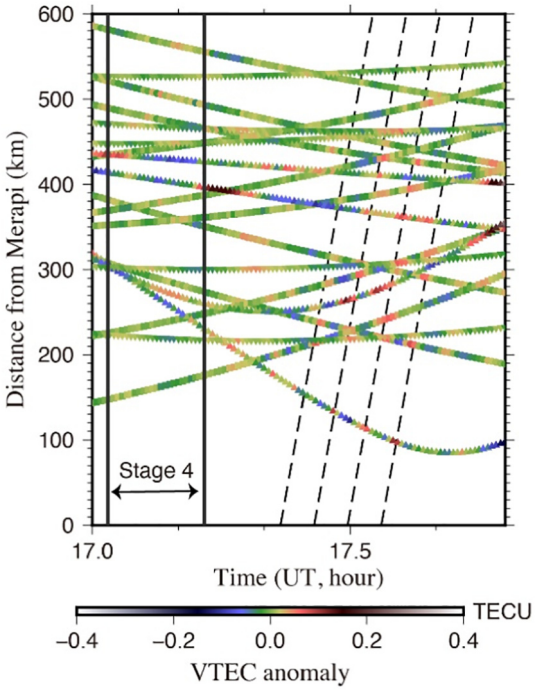

Fig. 6. Distance-time diagram of the ionospheric disturbance after the stage 4 of the 2010 Merapi eruption based on the GPS satellite 18, 25, 29 and 30 and stations located to the west or northwest of the volcano. The positive peak of ionospheric variation (shown in red) as shown in Fig. 5 propagates with the apparent velocity of ~0.8 km s^{-1} (dashed lines). (For interpretation of the references to colour in this figure legend, the reader is referred to the web version of this article.)

Here we assume that relative amplitude of TEC oscillation is proportional to the volume ejected in a unit time, often called mass eruption rate (MER). To test its validity, we compare the TEC amplitudes with the published values of MER for the three eruptions (Fig. 8a). The TEC oscillation amplitudes for the 2014 Kelud eruption is nearly twice as large as the other two, and this is consistent with the higher MER values of the Kelud eruption (3–4 × 10^7 kg s^{-1}) inferred with numerical simulations for its Plinian eruption on 13 February by Suzuki and Iguchi (2019) than the other two. The average MERs are estimated as ~10^7 kg s^{-1} for the stage 4 of the 2010 Merapi (Komorowski et al., 2013) and as 0.08–2.4 × 10^7 kg s^{-1} for the stages 3 and 4 of the 2015 Calbuco (Van Eaton et al., 2016) eruptions from the amount of the deposits.

This idea can be further confirmed by comparing the products of the relative oscillation intensity and the oscillation duration with the total volume of the deposit by the eruption. The duration is ~20 min for the 2010 Merapi eruption. The oscillation continued over an interval of ~120 min for the 2014 Kelud eruption (see Fig. 2 of Nakashima et al., 2016). The 2015 Calbuco eruption occurred as two episodes, and we assumed the total duration 450 min.

Fig. 8b compares the total amount of the volume of ejecta by the three eruptions studied here. For the 2010 Merapi eruption, it is reported as ~36.3 × 10^6 m^3, with >70% of this volume deposited during the stage 4 (Charbonnier et al., 2013). In the figure, we attached an error bar assuming the true volume is between 70 and 100% of this value. For the 2014 Kelud eruption, the total bulk deposit volume is estimated as 220 × 10^6 m^3 (Hidayati et al., 2018) or 250–500 × 10^6 m^3 (Maeno et al., 2019). For the 2015 Calbuco eruption, we used the value 560 ± 280 × 10^6 m^3 by Van Eaton et al. (2016). Fig. 8 suggests that total volume of the deposits is roughly proportional to the index defined as the product of relative TEC osillation amplitude and the oscillation duration.

The GNSS-TEC technique has several drawbacks. First of all, we need continuous GNSS stations around volcanoes and the technique can be used only for recent eruptions. The June 1991 Pinatubo eruption is considered to have MER as large as 10^9 kg s^{-1} (Suzuki and Koyaguchi, 2009). Fig. 8a suggests that

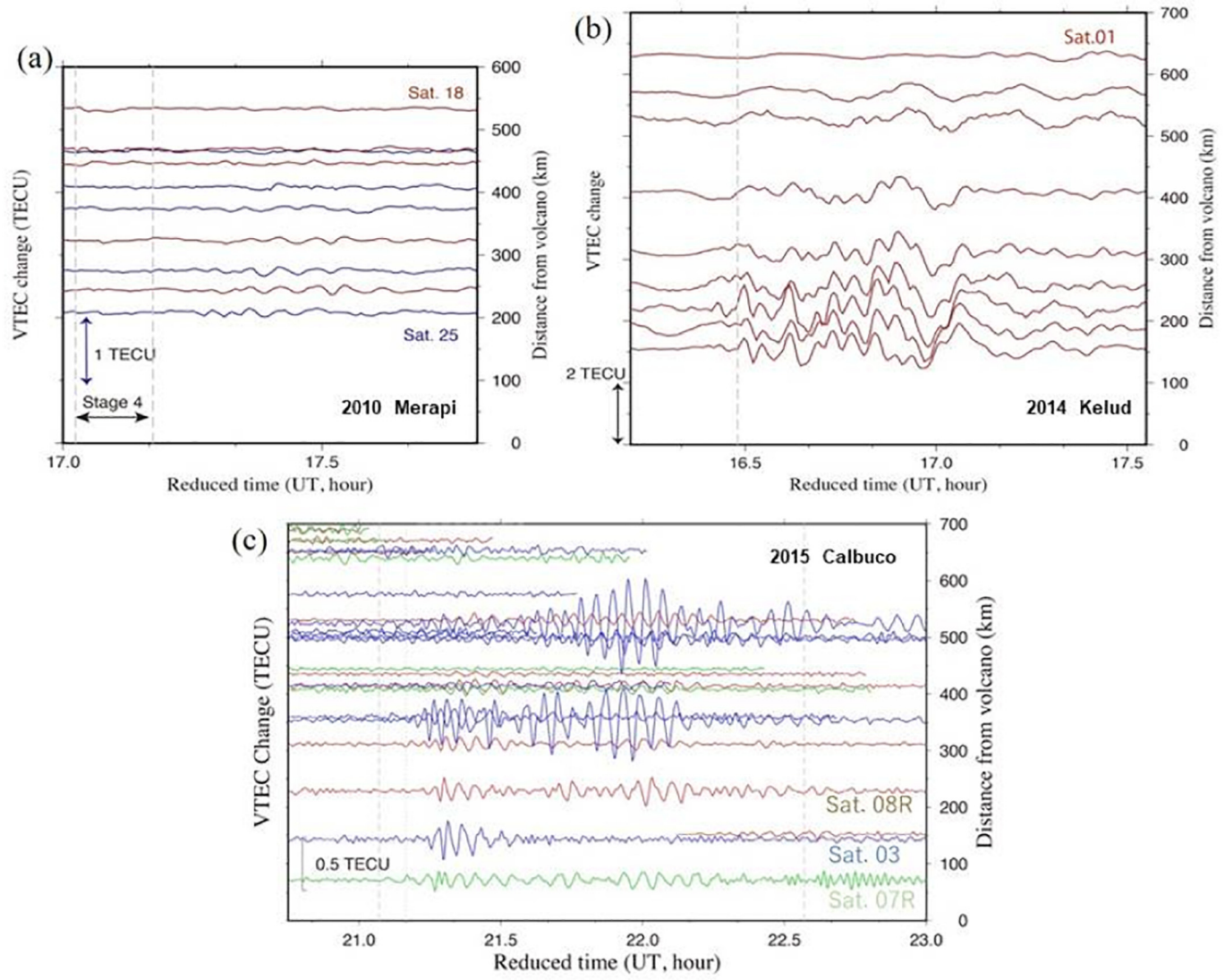

Fig. 7. Comparison of the ionospheric disturbance amplitudes of the two Indonesian cases, (a) 2010 Merapi, (b) the 2014 Kelud, and (c) the 2015 Calbuco (first eruption episode on 22 April) eruptions. Time axes are shifted backward to the volcanoes assuming 0.8 km s^{-1} propagating speed so that the TECs for different satellite-station pairs oscillate in phase. The vertical dashed line in (b) indicate the onset of the TEC oscillation, and the two vertical dashed lines in (c) indicate the period of the continuous eruption. In (c), we used the RAMSAC stations with SIPs located to the north of the volcano, and the distance from the volcano (right axis) is calculated at 21:10 (vertical dashed line). Average peak-to-peak amplitudes and their uncertainties are derived using the first 20 min of the oscillation using the satellite-station pair with the distance from the volcano around 200 km.

there were ultra-strong TEC oscillation signals if GNSS receivers were available at that time. Unfortunately, near-field observation data of the harmonic TEC oscillation are not available, although a longer period (~20 min) TEC oscillations, possibly due to internal gravity waves, were observed during 12–15 June by receiving microwave signals from a geostationary satellite in Taiwan (Cheng and Huang, 1992).

Another drawback is that the amplitudes of TEC oscillation are sensitive to the geometry of LoS, wave front, and the geomagnetic field, and it is difficult to compare the TEC oscillations for different eruptions with exactly the same condition. Nevertheless, ionospheric disturbances provide useful information on intensive volcanic eruptions. In real time, TEC can be monitored from GNSS stations hundreds of kilometers away from the volcano (Fig. 7). Amplitudes of the harmonic oscillation of TEC would offer a rough estimate of MER of the ongoing eruption in minutes. After the eruptions, the products of the oscillation amplitudes and the durations would offer a new scale, independent from conventional VEI, for estimating the total volume of deposits by Plinian eruptions. This would be useful especially when geological approaches are difficult.

CRediT authorship contribution statement

Mokhamad Nur Cahyadi: Conceptualization, Methodology, Formal analysis, Investigation, Supervision. **Ririn Wuri Rahayu:** Writing - original draft, Methodology, Formal analysis. **Kosuke Heki:** Conceptualization, Methodology, Formal analysis, Writing - review & editing, Supervision. **Yuki Nakashima:** Formal analysis, Investigation.

Declaration of competing interest

The authors declare that they have no known competing financial interests or personal relationships that could have appeared to influence the work reported in this paper.

Acknowledgements

We thank World Class Professor and PDUPT Research Program of Kemenristek BRIN-Indonesia 2019 for financial supports. Constructive comments by the two anonymous referees improved the quality of the paper.

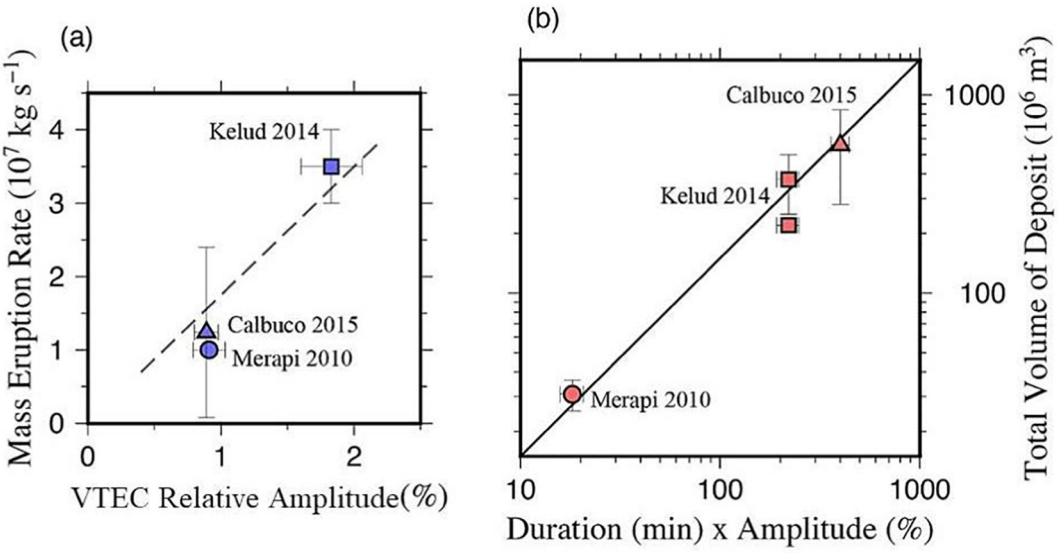

Fig. 8. (a) Comparison of the relative VTEC oscillation amplitudes and MERs of the 2010 Merapi (Komorowski et al., 2013), 2015 Calbuco (Van Eaton et al., 2016), and the 2014 Kelud (Suzuki and Iguchi, 2019) eruptions. (b) Comparison of the products of the ionospheric disturbance amplitudes and the durations, with the total volume of the deposits of the 2010 eruption of the Merapi volcano (Charbonnier et al., 2013), 2014 eruption of the Kelud volcano (Hidayati et al., 2018; Maeno et al., 2019), and the 2015 eruption of the Calbuco volcano (Van Eaton et al., 2016).

References

Astafyeva, E., 2019. Ionospheric detection of natural hazards. Rev. Geophys. 57, 1265–1288. https://doi.org/10.1029/2019RG000668.

Cahyadi, M.N., Heki, K., 2013. Ionospheric disturbances of the 2007 Bengkulu and the 2005 Nias earthquakes, Sumatra, observed with a regional GPS network. J. Geophys. Res. 118, 1–11. https://doi.org/10.1002/jgra.50208.

Cahyadi, M.N., Heki, K., 2015. Coseismic ionospheric disturbance of the large strike-slip earthquakes in North Sumatra in 2012: M_w dependence of the disturbance amplitudes. Geophys. J. Int. 200, 116–129.

Calais, E., Minster, J.B., Hofton, M.A., Hedlin, H., 1998. Ionospheric signature of surface mine blasts from Global Positioning System measurements. Geophys. J. Int. 132, 191–202.

Carr, B.B., Clarke, A.B., Vitturi, M.D.M., 2020. Volcanic conduit controls on effusive-explosive transitions and the 2010 eruption of Merapi Volcano (Indonesia). J. Volcanol. Geothermal Res. 392, 106767.

Charbonnier, S.J., Germa, A.M., Connor, C.B., Gertisser, R., Preece, K., Komorowski, J.-C., Lavigne, F., Dixon, T.H., Connor, L.J., 2013. Evaluation of the impact of the 2010 pyroclastic density currents at Merapi volcano from high-resolution satellite imagery analysis, field investigations and numerical simulations. J. Volcanol. Geotherm. Res. 261, 295–315.

Cheng, K., Huang, Y.N., 1992. Ionospheric disturbances observed during the period of Mount Pinatubo eruptions in June 1991. J. Geophys. Res. 97, 16995–17004. https://doi.org/10.1029/92JA01462.

Choosakul, N., Saito, A., Iyemori, T., Hashizume, M., 2009. Excitation of 4-min periodic ionospheric variations following the great Sumatra– Andaman earthquake in 2004. J. Geophys. Res. 114, A10313. https://doi.org/10.1029/2008JA013915.

Dabrowa, A.L., Green, D.N., Rust, A.C., Phillips, J.C., 2011. A global study of volcanic infrasound characteristics and the potential for long-range monitoring. Earth Planet. Sci. Lett. 310 (3), 369–379.

Dautermann, T., Calais, E., Mattioli, G.S., 2009a. Global Positioning System detection and energy estimation of the ionospheric wave caused by the 13 July 2003 explosion of the Soufrière Hills Volcano, Montserrat. J. Geophys. Res. 114, B02202. https://doi.org/10.1029/2008JB005722.

Dautermann, T., Calais, E., Lognonné, P., Mattioli, G.S., 2009b. Lithosphere-atmosphere-ionosphere coupling after the 2003 explosive eruption of the Soufriere Hills Volcano, Monserrat. Geophys. J. Int. 179, 1537–1546. https://doi.org/10.1111/j.1365-246X.2009.04390.x.

Heki, K., 2006. Explosion energy of the 2004 eruption of the Asama Volcano, central Japan, inferred from ionospheric disturbances. Geophys. Res. Lett. 33, L14303. https://doi.org/10.1029/2006GL026249.

Heki, K., 2020. Chapter 5-3: ionospheric disturbances related to earthquakes. In: Huang, C., Lu, G. (Eds.), Advances in Ionospheric Research: Current Understanding and Challenges, Space Physics and Aeronomy. vol. Volume 3. Wiley/American Geophysical Union, p. 320 (ISBN:978-1-119-50755-0.o).

Hidayati, S., Triastuty, H., Mulyana, I., Adi, S., Ishihara, K., Basuki, A., Kuswandarto, H., Priyanto, B., Solikhin, A., 2018. Differences in the seismicity preceding the 2007 and 2014 eruptions of Kelud volcano, Indonesia. J. Volcanol. Geothermal Res. 382, 50–67.

Hofmann-Wellenhof, B., Lichtenegger, H., Wasle, E., 2008. GNSS-Global Navigation Satellite Systems. Springer https://doi.org/10.1007/978-3-211-73017-1.

Jousset, P., Pallister, J., Surono, 2013. Merapi eruption, special issue of. J. Volcanol. Geothermal Res. 261, 1–388.

Kanamori, H., Mori, J., Harkrider, D.G., 1994. Excitation of atmospheric oscillations by volcanic eruptions. J. Geophys. Res. 99, 21,947–21,961. https://doi.org/10.1029/94JB01475.

Komorowski, J.-C., Jenkins, S., Baxter, P.J., Picquout, A., Lavigne, F., Charbonnier, S., Gertisser, R., Preece, K., Cholik, N., Budi-Santoso, A., Surono, 2013. Paroxysmal dome explosion during the Merapi 2010 eruption: Processes and facies relationships of associated high-energy pyroclastic density currents. J. Volcanol. Geothermal Res. 261, 260–294.

Maeno, F., Nakada, S., Yoshimoto, M., Shimano, T., Hokanishi, N., Zaennudin, A., Iguchi, M., 2019. A sequence of a plinian eruption preceded by dome destruction at Kelud volcano, Indonesia, on February 13, 2014, revealed from tephra fallout and pyroclastic density current deposits. J. Volcanol. Geothermal Res. 382, 24–41.

Matoza, R., Fee, D., Green, D., Mialle, P., 2019. Volcano infrasound and the international monitoring system. In: Le Pichon, A., Blanc, E., Hauchecorne, A. (Eds.), Infrasound Monitoring for Atmospheric Studies. Springer, Cham, pp. 1023–1077 (ISBN:978-3-319-75138-2).

Nakashima, Y., 2018. Multi-Sensor Study of Dynamics of Atmospheric Waves Induced by Volcanic Eruptions. PhD Thesis. Hokkaido University.

Nakashima, Y., Heki, K., Takeo, A., Cahyadi, M.N., Aditiya, A., Yoshizawa, K., 2016. Atmospheric resonant oscillations by the 2014 eruption of the Kelud volcano, Indonesia, observed with the ionospheric total electron contents and seismic signals. Earth Planet. Sci. Lett. 434, 112–116. https://doi.org/10.1016/j.epsl.2015.11.029.

Nishida, K., Kobayashi, N., Fukao, Y., 2000. Resonant oscillation between the solid earth and the atmosphere. Science 287, 2244–2246.

Occhipinti, G., Rolland, L., Lognonné, P., Watada, S., 2013. From Sumatra 2004 to Tohoku-oki 2011: the systematic GPS detection of the ionospheric signature induced by tsunamigenic earthquakes. J. Geophys. Res. Space Phys. 118, 3626O. https://doi.org/10.1002/jgra.50322.

Rideout, W., Coster, A., 2006. Automated GPS processing for global total electron 246 content data. GPS Solut 10, 219–228.

Rolland, L., Lognonné, P., Astafyeva, E., Kherani, A., Kobayashi, N., Mann, M., Munekane, H., 2011. The resonant response of the ionosphere imaged after the 2011 Tohoku-oki earthquake. Earth Planets Space 63, 853–857. https://doi.org/10.5047/eps.2011.06.020.

Rolland, L.M., Vergnolle, M., Nocquet, J.-M., Sladen, A., Dessa, J.-X., Tavakoli, F., Nankali, H.R., Cappa, F., 2013. Discriminating the tectonic and non-tectonic contributions in the ionospheric signature of the 2011, Mw7.1, dip-slip Van earthquake, Eastern Turkey. Geophys. Res. Lett. 40, 2518–2522. https://doi.org/10.1002/grl.50544.

Romero, J.E., Morgavi, D., Arzilli, F., Daga, R., Caselli, A., Reckziegel, F., Viramonte, J., Alvarado, J.D., Polacci, M., Burton, M., Perugini, D., 2016. Eruption dynamics of the 22–23 April 2015 Calbuco Volcano (Southern Chile): analyses of tephra fall deposits. J. Volcanol. Geothermal Res. 317, 15–29.

Saito, A., Tsugawa, T., Otsuka, Y., Nishioka, M., Iyemori, T., Matsumura, M., Saito, S., 2011. Acoustic resonance and plasma depletion detecte d by GPS total electron content observation after the 2011 off the Pacific coast of Tohoku Earthquake. Earth Planets Space 63, 863–867.

Shults, K., Astafyeva, E., Adourian, S., 2016. Ionospheric detection and localization of volcano eruptions on the example of the April 2015 Calbuco events. J. Geophys. Res. Space Physics 121, 10,303–10,315. https://doi.org/10.1002/2016JA023382.

Surono, M., Jousset, P., Pallister, J., Boichu, M., Buongiorno, M.F., Budisantoso, A., Rodriguez, F.C., Andreastuti, S., Prata, F., Schneider, D., et al., 2012. The 2010 explosive

eruption of Java's Merapi volcano – a '100-year' event. J. Volcanol. Geothermal Res. 241-242, 121–135.
Suzuki, Y.J., Iguchi, M., 2019. Determination of the mass eruption rate for the 2014 Mount Kelud eruption using three-dimensional numerical simulations of volcanic plumes. J. Volcanol. Geothermal Res. 382, 42–49.
Suzuki, Y.J., Koyaguchi, T., 2009. A three-dimensional numerical simulation of spreading umbrella clouds. J. Geophys. Res. Solid Earth 114, B03209. https://doi.org/10.1029/2007JB005369.
Tahira, M., 1995. Acoustic resonance of the atmospheric at 3.7 mHz. J. Atmos. Sci. 52, 2670–2674.
Van Eaton, A.R., Amigo, A., Bertin, D., Mastin, L.G., Glacosa, R.E., Gonzalez, J., Valderrama, O., Fontijn, K., Behnke, S.A., 2016. Volcanic lightning and plume behavior reveal evolving hazards during the April 2015 eruption of Calbuco volcano, Chile. Geophys. Res. Lett. 43, 3563–3571.
Watada, S., Kanamori, H., 2010. Acoustic resonant oscillations between the atmosphere and the solid earth during the 1991 Mt. Pinatubo eruption. J. Geophys. Res. 115, B12319. https://doi.org/10.1029/2010JB007747.